Absolute, Cascade-Free Cross Sections for the $^2S \rightarrow {}^2P$ Transition in Zn^+ Using Electron-Energy-Loss and Merged-Beams Methods

Steven J. Smith,[1] K-F. Man,[1] R. J. Mawhorter,[2] I. D. Williams,[3] and A. Chutjian[1]

[1]*Jet Propulsion Laboratory, California Institute of Technology, Pasadena, California 91109*

[2]*Department of Physics and Astronomy, Pomona College, Claremont, California 91711*

[3]*Department of Pure and Applied Physics, Queens University, Belfast, BT7 INN, United Kingdom*

(Received 22 October 1990; revised manuscript received 20 February 1991)

Absolute, cascade-free excitation cross sections in an ion have been measured for the resonance $^2S \rightarrow {}^2P$ transition in Zn^+ using electron-energy-loss and merged electron-ion beams methods. Measurements were carried out at electron energies of below threshold to 6 times threshold. Comparisons are made with 2-, 5-, and 15-state close-coupling and distorted-wave theories. There is good agreement between experiment and the 15-state close-coupling cross sections over the energy range of the calculations.

PACS numbers: 34.80.Kw, 35.80.+s

Excitation of ions by electron impact plays an important role in a variety of plasmas ranging from solar and stellar atmospheres to the interstellar medium, planetary ionospheres and magnetospheres, confined-fusion plasmas, and x-ray lasers [1,2]. Modeling of these plasmas has involved the use of calculated collision strengths to extract an electron density or temperature from an optically measured emission-line ratio. There are, with the exception of some recent results in Si^{3+} at threshold [3], no experimental cascade-free absolute cross sections at energies significantly above threshold which could serve to test theory, or the semiempirical Gaunt-factor approximation sometimes used to provide missing data.

We report herein use of the electron-energy-loss technique [4,5] in a merged-beams geometry [3,6] to measure absolute excitation cross sections in Zn^+, an ion for which theoretical [7–10] and experimental photon-emission [11] cross sections are available. Extensions to multiply charged ion targets are possible in a relatively straightforward way. Measurements were made at electron energies from below threshold (at 6.05 eV) to 37.5 eV, or approximately 6 times threshold. This is a critical energy regime since (a) electron-ion cross sections have their maximum at threshold, (b) theoretical calculations are difficult, and (c) in many types of plasmas, one has a maximum in the electron energy distribution function in the range 1–50 eV, so that line excitation rates are a maximum.

A schematic diagram of the apparatus used in these measurements is shown in Fig. 1 [6]. Briefly, a beam of electrons is merged with a beam of ions in a uniform, stable solenoidal magnetic field through the use of trochoidal ($\mathbf{E}\times\mathbf{B}$ fields) deflection plates (MP). Inelastically scattered electrons from the interaction region are demerged by a second set of trochoidal plates (AP) which disperse the electrons according to their final longitudinal and radial velocities. A third set of deflection plates (DP) is used to deflect the parent electron beam out of the plane of the experiment (defined by the merging and analyzing directions) prior to collection in its Faraday cup. This is done to minimize electron background arising from incomplete collection. The merging and analyzing $\mathbf{E}$ fields are chosen to minimize beam-shear effects [12], while having only a small deflection effect upon the 4- keV ion beam. The magnetic-field strength is typically 50 G, and the electric field is $\sim$60 V/cm (depending on electron energy).

The resulting energy-loss feature is detected using a microchannel-plate array and two-dimensional resistive anode as a position-sensitive detector (PSD) facing into the beams direction. A wire mesh is placed in front of the PSD to allow discrimination, via retarding potentials, between high- and low-energy electrons (see below). A PC/CAMAC system is used for data acquisition and control. Data are stored in a histogramming memory at the output of the PSD. The cross section $\sigma(E)$ at the center-of-mass (c.m.) energy E is related to the experi-

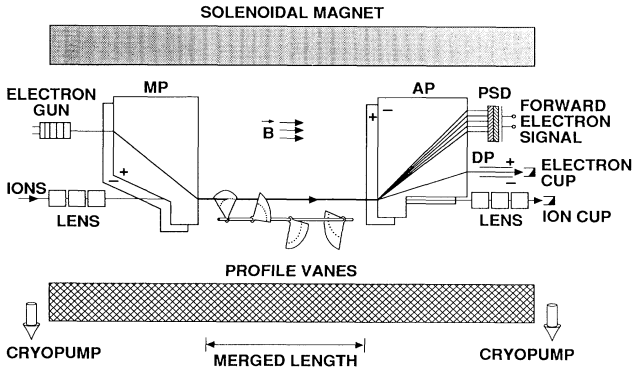

FIG. 1. Schematic diagram of the merged-beams apparatus. Electrons are merged onto the ion beam by trochoidal plates MP, and analyzed by plates AP. The parent electron beam is deflected out of the experimental plane by the plates DP. Signal detection is by means of the position-sensitive detector (PSD).

mental parameters by the relation

$$\sigma(E) = \frac{Re^2F}{\epsilon I_i I_e L}\left|\frac{v_e v_i}{v_e - v_i}\right|, \quad (1)$$

where R is the signal rate ($\sec^{-1}$), e the electron charge, I_e and I_i the electron and ion currents (in A), respectively, L the merged path length (in cm), v_e and v_i the electron and ion velocities (in cm/sec), respectively, ϵ the detection efficiency of the PSD (dimensionless), and F the overlap factor between the electron and ion beams (in cm^2). A double-beam modulation technique is used, and the rate R is obtained from the net inelastic signal divided by the total "on" time of the experiment. This time is read from the accumulated clock pulses in a quad-scaler-clock triggered by the beams' modulation circuitry. The overlap factor F is measured at four fixed positions along the merged length by rotating vanes which sweep through the two beams and scan their profiles by a series of nine 0.3-mm-diam holes per vane [13]. The vanes are swept by a PC-controlled microstep motor. Electron and ion currents are simultaneously read and stored through separate charge digitizers. Typical operating conditions are $I_e \sim 0.15$ nA, $I_i \sim 20$ nA, $R \sim 10$–100 Hz, and beam diameters ~ 1 mm. Typical background rates are 5–10 kHz (electrons), 2–5 kHz (ions), and 3–30 Hz (Coulomb scattering). The merged interaction length is $L = 20$ cm. The PSD detection efficiency is $\epsilon = 0.836 \pm 0.011$ as measured by comparing electron rates over the face of the PSD and currents in a Faraday cup as measured by a stable, high-sensitivity electrometer. Pressure in the merged region during operation of both beams was 2.7×10^{-7} Pa.

A number of diagnostic tests were made on the data to verify the results. At the 5% uncertainty level, $\sigma(E)$ was found to be independent of beam modulation frequency, beam currents, separate beam energies giving the same c.m. energy, electron count rate, and beam overlap factor. Measurements taken below threshold gave zero cross section. This indicated that backgrounds arising from the ion and electron beams and electronic noise were being subtracted correctly, and that there was a negligible metastable Zn^+ component in the beam. Special attention was given to the energy range 6.0–8.5 eV to search for a contribution from the onset of the $4s\,^2S \rightarrow 4s^2\,^2D$ transition. None was found, and hence the ^2D contribution is negligible at the 5% uncertainty level. No search was made for the $4s\,^2S \rightarrow 5s\,^2S$ transition at 10.97 eV since (a) the residual energy of electrons having excited this transition is even smaller than that of the possibly competing $S \rightarrow D$ transition, and hence the spectrum would fall on a different part of the PSD; (b) because of the optically forbidden $S \rightarrow S$ symmetry, one expects the integral cross section to be smaller, leading to a weaker signal on the PSD; and (c) because of this forbiddenness, one also expects the differential cross section (DCS) to be less forward peaked, leading to a spatially broader signal on the PSD. Finally, using the SIMION charged-particle field and trajectory code [14] we noticed that, at the highest energies, inelastically scattered electrons could possibly "scrape" the positive analyzer plate at the B field (42 G) then in use. A number of measurements were repeated at a higher field (55 G), and these showed no significant deviation from earlier data.

One other interfering effect is worthy of note: Elastically scattered (Coulomb) electrons at large scattering angles up to 90° can have a longitudinal velocity comparable to that of electrons inelastically scattered in the forward direction. These Coulomb electrons would occupy the same position on the PSD, and could be counted in the net signal. Using the SIMION code, calculations of electron trajectories were carried out in the present apparatus geometry and configuration of electric and magnetic fields. Electron trajectories were calculated in two limiting cases of incident energy (near threshold, and at 6 times threshold), over a range $(0, 3\pi/2)$ of starting azimuthal angles ϕ and over a range of polar angles θ. A "footprint area" of the inelastic feature of the PSD was simulated, as well as of the underlying Coulomb background, from more than 100 trajectories over the range of θ and ϕ. Combining this area with the DCS at that θ, as obtained from the 5-state close-coupling (5CC) results [7,8], a "density map" was obtained (the cross section between θ and $\theta + d\theta$ divided by the footprint area at θ). Many density maps were made to cover the entire range of θ contributing to the scattering. These resultant maps included beam shear by displacing the starting electron trajectories 0.5 mm up and 0.5 mm down from the merged-beams center line. Then separately for the inelastic feature and Coulomb background the density maps were combined and integrated numerically over θ to give a profile of density versus position on the PSD. This final profile is a simulation of what the PSD actually "sees."

The results can be summarized as follows: Close to threshold, the energies of the Coulomb and inelastically scattered electrons are far apart, so that only high-angle Coulomb scattering enters the grids. This high-angle differential cross section is small, and hence the elastic signal is weak (because of the smaller cross section), and is spread along the PSD (because of the larger-gyroradii electrons), while the inelastic feature (an optically allowed transition) corresponds to a larger, forward-peaked cross section. The latter is concentrated in a spot determined by beam size, shear, and angular distribution. We select a "sufficiently large" pixel area that just includes the inelastic peak and eliminates outlying Coulomb scattering. During data analysis we also select a base-line level that subtracts off most of the smooth, underlying Coulomb contribution beneath the inelastic peak. The pixel area and base-line level are varied to determine the sensitivity of these final cross sections to the parame-

ters.

In actual practice, the wire grid in front of the PSD is first biased dc negative to reflect the inelastically scattered component and transmit the elastically scattered component. The mesh is then biased more positively in a second measurement to transmit the inelastically and the underlying elastically scattered electrons. The net signal rate R is then found by recording counts at the two grid biases, within the preset pixel area and threshold level, and taking the difference.

Away from threshold, the residual energies of the inelastic and Coulomb-scattered electrons are closer, so the underlying Coulomb contribution shrinks in pixel area, as does the inelastic footprint. While the DCS's become more forward peaked, both the SIMION calculations and the error incurred in the Coulomb subtraction is approximately 7%, and decreases closer to threshold. The final errors in the absolute cross sections include an estimate of error incurred in this subtraction. Further details of the simulations will be given in a longer publication.

Present absolute electron excitation cross sections for the $4s\ ^2S \rightarrow 4p\ ^2P$ transition in Zn^+ are shown in Fig. 2. With the use of a single PSD in the forward direction, one measures only the forward (0°–90°, c.m. frame) portion of the differential electron-scattering cross section. While this represents for an optically allowed transition the major part of the integral cross section [4,5], an estimate is nevertheless required for the 90°–180° contribution. This was obtained from the 15-state (15CC) calculations [9], and served to raise the cross section by factors of 1.31, 1.24, 1.13, 1.08, and 1.025 at energies of 7.9, 10.2, 12.6, 14.0, and 30.0 eV, respectively. (It is also interesting to note that measurements at threshold are made possible by the small kinematic effect of electrons and ions moving in the same direction: Electrons that have excited the $^2S \rightarrow {}^2P$ transition at threshold still have $\sim$1 eV energy in the laboratory frame, and hence are detected on the PSD.)

The error limits on the absolute cross section are 17% at the 90% confidence level, and represent the quadrature-combined errors in the form factor (6%), choice of base line and pixel area (7%), dead-time correction (3%), detector calibration (2%), beam currents (1% each), and merged path length (1%). The uncertainties in electron energy and the energy resolution are 0.2 and 0.3 eV (FWHM), respectively.

Also shown in Fig. 2 are line-emission cross sections (open squares) [11], 15CC calculations (dashed line) [9], 5CC calculations both with (open triangles) and without (open diamonds, asterisks) cascade into the ^2P level [7,8], 2CC calculations (half-filled diamonds) [8], and distorted-wave calculations (open plus signs) [10]. Only the 15CC theory includes the effects of resonances. The Gaunt-factor approximation (divided by 3, with $f = 0.732$) is given as the solid line [15]. The present results are in good agreement with the line-emission results

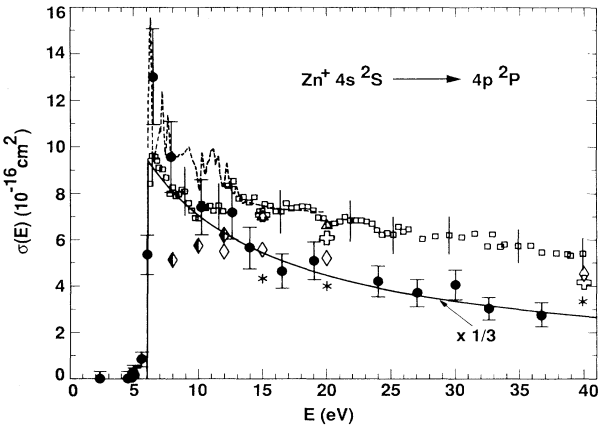

FIG. 2. Absolute cross sections for excitation of the $4s\ ^2S \rightarrow 4p\ ^2P$ transition in Zn^+. Present, cascade-free results are given as solid circles, and line-emission cross sections [11] as open squares. 15CC calculations (dashed line) are from Ref. [9], 5CC calculations are from Refs. [7] and [8], both with (open triangles) and without (open diamonds, asterisks) cascade, 2CC results (half-filled diamonds) are from Ref. [8], and distorted-wave calculations (open plus signs) are from Ref. [10]. The Gaunt-factor approximation, divided by a factor of 3, is given by the solid line [15].

near threshold and, as expected, lie below these results at energies above threshold where cascade becomes significant (opening of the $5s\ ^2S$ level at 11.0 eV). The agreement of the various close-coupling calculations among themselves is a question of wave function, inclusion of resonances, number of coupled channels, etc. This is a fairly involved matter, and will be resolved by the theoreticians in a future publication [16]. The agreement of present experiments with the 15CC calculations is very good at energies between threshold and 14 eV. (The theoretical 15CC curve was shifted by 0.35 eV to higher energies so that calculated and spectroscopic thresholds would coincide.) The 15CC results are somewhat flat between 14 and 20 eV. Their good agreement with the photon-emission data [11] (cascade present) would indicate that cascading is negligible. This result appears inconsistent with the cascade contribution calculated in Ref. [7] (see Fig. 2). In addition, there is also very good agreement between the present experiment and the 5CC results (open diamonds) to 20 eV, above which experiment falls slightly below both close-coupling and distorted-wave results and follows more closely the shape of the Gaunt-factor curve. It is interesting to point out that experiment is consistent with the small effects of resonances at threshold calculated in the 15CC, which are analogous to *ab initio* close-coupling calculations, including resonances, of the $^2S \rightarrow {}^2P$ excitation cross section in Cu (isoelectronic with Zn^+ [17]).

This work was carried out at the Jet Propulsion Laboratory, California Institute of Technology, and was sup-

ported by the National Aeronautics and Space Administration, and the Lawrence Livermore National Laboratory Collaboration with the Queen's University of Belfast was made possible through a NATO International Collaborative Research Grant. Several of us (S.J.S., K-F.M., R.J.M., and I.D.W.) acknowledge support from the NASA National Research Council for Resident Research Associateships at the Jet Propulsion Laboratory. We are grateful to R. J. W. Henry and M. S. Pindzola for their calculated cross sections prior to publication, and to P. O. Egan for many helpful discussions.

[1] See, for example, the separate reviews by A. Dalgarno, D. E. Post, and D. H. Crandall, in *Physics of Ion-Ion and Electron-Ion Collisions,* edited by F. Brouillard and J. W. McGowan (Plenum, New York, 1983).

[2] W. H. Goldstein, B. L. Whitten, A. U. Hazi, and M. H. Chen, Phys. Rev. A **36**, 3607 (1987).

[3] E. K. Wåhlin, J. S. Thompson, G. H. Dunn, R. A. Phaneuf, D. C. Gregory, and A. C. H. Smith, Phys. Rev. Lett. **66**, 157 (1991).

[4] A. Chutjian, A. Z. Msezane, and R. J. W. Henry, Phys. Rev. Lett. **50**, 1357 (1983).

[5] I. D. Williams, A. Chutjian and R. J. Mawhorter, J. Phys. B **19**, 2189 (1986).

[6] R. J. Mawhorter, I. D. Williams, B. F. Lewis, and A. Chutjian, Bull. Am. Phys. Soc. **32**, 1273 (1987); in Proceedings of the Twelfth International Conference on Atomic Physics, Ann Arbor, Michigan, 1990 (AIP, New York, to be published).

[7] A. Z. Msezane and R. J. W. Henry, Phys. Rev. A **25**, 692 (1982).

[8] R. J. W. Henry (private communication) (2CC).

[9] M. S. Pindzola (private communication) (15CC).

[10] A. W. Pangantiwar and R. Srivastava, J. Phys. B **21**, L219 (1988).

[11] W. T. Rogers, G. H. Dunn, J. O. Olsen, M. Reading, and G. Stefani, Phys. Rev. A **25**, 681 (1982).

[12] M. R. McMillan and J. H. Moore, Rev. Sci. Instrum. **51**, 944 (1980).

[13] D. E. Nitz, M. W. Geis, K. A. Smith, and R. D. Rundel, Rev. Sci. Instrum. **47**, 306 (1976).

[14] D. A. Dahl and J. E. Delmore, Idaho National Engineering Laboratory Report No. EGG-CS-7233 Rev. 2 (unpublished).

[15] R. Mewe, Astron. Astrophys. **20**, 215 (1972).

[16] N. R. Badnell, D. C. Griffin, R. J. W. Henry, M. S. Pindzola, and W. L. van Wyngaarden (to be published).

[17] K. F. Scheibner, A. U. Hazi, and R. J. W. Henry, Phys. Rev. A **35**, 4869 (1987).